crystals

MDPI

Article

Geochemistry and Genesis of Magnesium Tourmalines in Jian Forsterite Jade Deposits from Ji'an County, Jilin Province, Northeast China

Huaimou Yang [1,2], Mingyue He [1,2,*], Mei Yang [2,3], Bijie Peng [1,2], Shaokun Wu [1,2] and Yujia Shi [1,2]

1 School of Gemmology, China University of Geosciences, Beijing 100083, China; yanghuaimou@email.cugb.edu.cn (H.Y.); 3009200003@email.cugb.edu.cn (B.P.); 3009210005@email.cugb.edu.cn (S.W.); 3009220006@email.cugb.edu.cn (Y.S.)
2 The National Mineral Rock and Fossil Specimens Resource Center, China University of Geosciences, Beijing 100083, China; yangmei@cugb.edu.cn
3 Sciences Institute, China University of Geosciences, Beijing 100083, China
* Correspondence: hemy@cugb.edu.cn

Abstract: The Jian forsterite jade, so named because of its enrichment in end-member forsterite, is a new type of jade found in Ji'an County (Jilin Province, Northeast China). Tourmaline is discovered in Jian forsterite jade deposits and is characterized by magnesium enrichment. In this study, three types of magnesium tourmaline were identified from the pegmatite veins (type 1), the contact zone (type 2), and the tourmaline veins in jade (type 3). The results are shown by the main test methods, such as EPMA, Micro-XRF, and LA-ICP-MS. The substitutions of $Fe^{2+}{}_{-1}Mg^{2+}{}_{-1}$, $(\square Al^{3+})_{-1}$ $(Na^{+}Mg^{2+})_{-1}$, $(\square Al^{3+}{}_{2})_{-1}$ $(Ca^{2+}R^{2+}{}_{2})_{-1}$, etc. are inferred by the variations in the major element compositions. From type 1 to type 2 tourmaline, the content of Mg, Sr, and Sn gradually increases, the content of Fe, Zn, K, Mn, Sc, Ga, and Co gradually decreases, the content of Ca initially decreases and then increases, and the content of Na initially increases and then decreases. Type 3 tourmaline has significantly higher Si and Al than the first two types, and the content of the remaining elements lies between the above two types. We propose that tourmalines in Jian forsterite jade deposits are typically of hydrothermal origins and are mainly constrained by magnesium, which is related to the contact metasomatic metamorphism of pegmatite-related hydrothermal fluid with the Jian forsterite jade, and the chemical composition of tourmaline indicates the fluid characteristics of gradual serpentinization of Jian forsterite jade.

Keywords: tourmaline; forsterite; Jian forsterite jade; geochemistry; trace element

Citation: Yang, H.; He, M.; Yang, M.; Peng, B.; Wu, S.; Shi, Y. Geochemistry and Genesis of Magnesium Tourmalines in Jian Forsterite Jade Deposits from Ji'an County, Jilin Province, Northeast China. *Crystals* **2023**, *13*, 1653. https://doi.org/10.3390/cryst13121653

Academic Editor: Sergey V. Krivovichev

Received: 17 November 2023
Revised: 27 November 2023
Accepted: 28 November 2023
Published: 30 November 2023

1. Introduction

Tourmaline is distributed in Jian forsterite jade deposits. The Jian forsterite jade is rich in forsterite, which is a new type of jade found in Ji'an County (Northeast China) [1–3]. Forsterite is capable of occurring in a variety of petrogenetic environments. But, olivine with Fo% > 96 (here called Fo% = 100 × Mg/[Mg + Fe], mol%) is not typical of igneous rocks, while olivine with Fo% > 99 is rare [4–6]. According to previous studies, forsterite can also be formed in various reaction processes, such as the dehydration reaction of serpentine, Mg–Fe exchange between olivine and chromite, the metamorphism of dolomite and limestone, etc. [7–9]. Unlike the previous study, the forsterite (Fo% > 99%) in Jian forsterite jade has a homogeneous composition and coexists with secondary phases, such as serpentine and brucite. However, the mechanism of the genesis of this particular forsterite is not well understood. It may be formed by fluid serpentinization of the ancient refractory lithospheric mantle of the North China Craton by a possible subduction plate dehydration process or by contact metamorphism between silica-rich fluids and Mg-rich dolomite [2,3].

Tourmaline is an effective indicator mineral for petrogenesis because it can exist in most rock types and has a wide range of P–T stability, which can record the characteristics of the rock evolution process at the time of its formation and contains a wealth of geological information [10–14]. Depending on the type of genesis, tourmaline can be mainly classified as magmatic, hydrothermal, and metamorphic [15–20].

In previous studies, the study of the genesis of the Jian forsterite jade was mainly developed by means of its chemical composition, spectroscopic characteristics, and oxygen isotopes [2,3]. A preliminary investigation of tourmaline in Jian forsterite jade deposits revealed its high magnesium content, but a systematic mineralogical characterization of this good indicator mineral and the indicative significance of its genesis has not been developed [21,22]. In addition, the lack of data on the magnesium-rich component of the Al–Mg–Fe diagram for defining the host rock environment of tourmaline has restricted the usefulness of magnesium-rich tourmaline in discriminating petrogenesis. Therefore, the data from studies on magnesium-rich tourmaline have the potential to modify and improve the boundaries of the diagram [23]. In this study, we focus on the geochemistry and genesis of magnesium tourmaline in Jian forsterite jade and analyze the chemical composition variations of different types of tourmaline to provide new ideas for investigating the genesis and evolution of this jade. The study also provides new data for the research of magnesium-rich tourmaline, which may be complementary to the petrogenetic indication significance of tourmaline.

2. Geological Setting

This study area is located in Ji'an County, Jilin Province, Northeast China and geotectonically lies in the north-central part of the Liao–Ji Proterozoic rift zone in the eastern part of the North China Craton [24–27]. This area lies in the east of the Songliao depression and consists of four major tectonic formations: the Ji–Hei orogenic belt (which has an N–NS trending), the Liao–Ji Proterozoic rift zone, the Longgang Block to the north, and the Langrim Block to the south (Figure 1).

Hornblende monzogranite (crystallization age is about 2.175 Ga) and porphyritic granites (crystallization age is about 1.875 Ga.) are major Paleoproterozoic granitoids in the Liao–Ji region [28]. The stratum exposed in this study area is mainly the Ji'an Group, and geochemical and petrological studies indicate that it may have formed in an active continental margin environment [29]. The Ji'an Group is now divided into the Mayihe, Huangchagou, and Dadongcha formations. The study area is located in the Mayihe Formation, which consists of altered felsitic and gneissic rocks, dolomitic marble, serpentinized olivine marble, serpentinite, and amphibolite [29–32]. Zircon U–Pb studies of the Ji'an metavolcanic and metamorphic rocks suggest that the Ji'an Formation formed at 2.2–2.0 Ga and then underwent regional metamorphism at 1.95–1.80 Ga [29,33].

The mine is an open pit, with the exposed ore body approximately 4455.0 m^2 (~66.0 m long and 67.5 m wide). The jade deposit is mainly blocky with secondary layers visible on the surface and yellow-green rock inside, and varying degrees of serpentinization have occurred (Figure 2). There are pegmatite veins interspersed in the jade deposit, and a variety of minerals, such as tourmaline, mica, and tremolite, are developed between the contact zone of the pegmatite and the jade ore body (Figure 3).

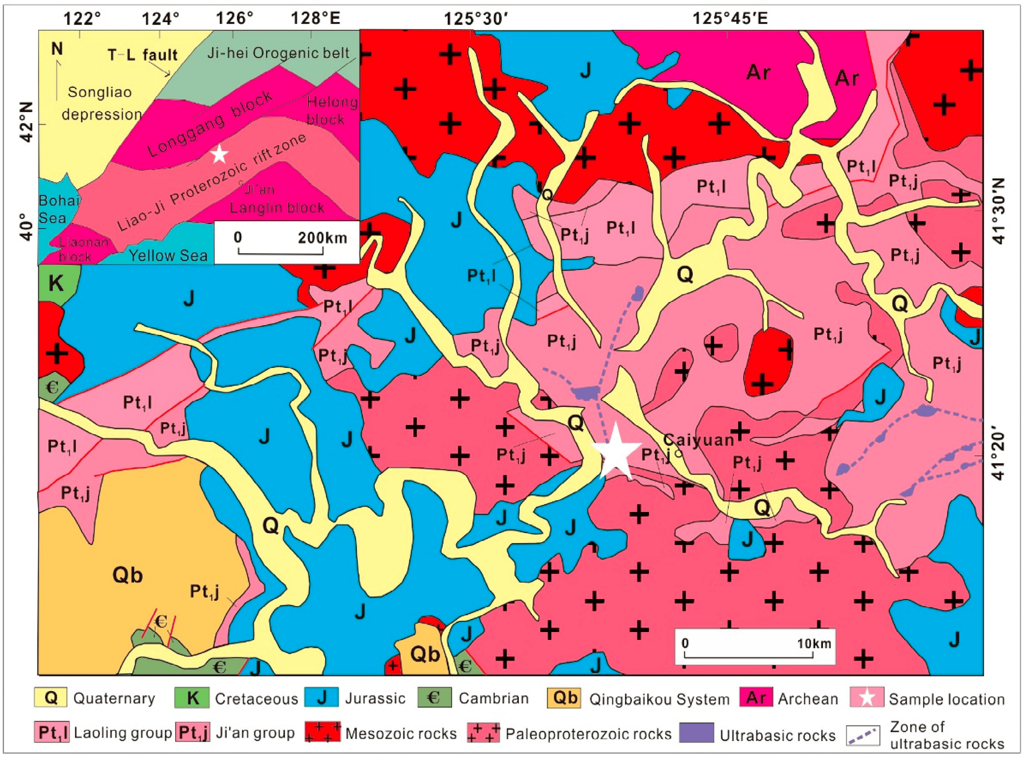

Figure 1. Geological map of the study area [2].

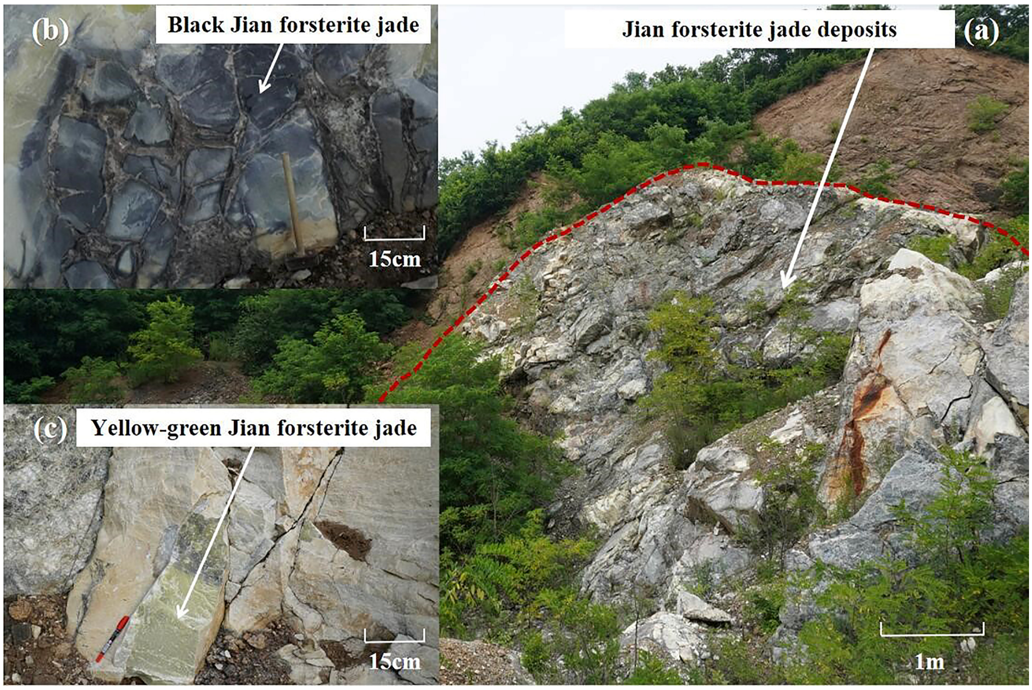

Figure 2. (**a**) Photographs of Jian forsterite jade deposits; (**b**) Black Jian forsterite jade; (**c**) Yellow-green Jian forsterite jade.

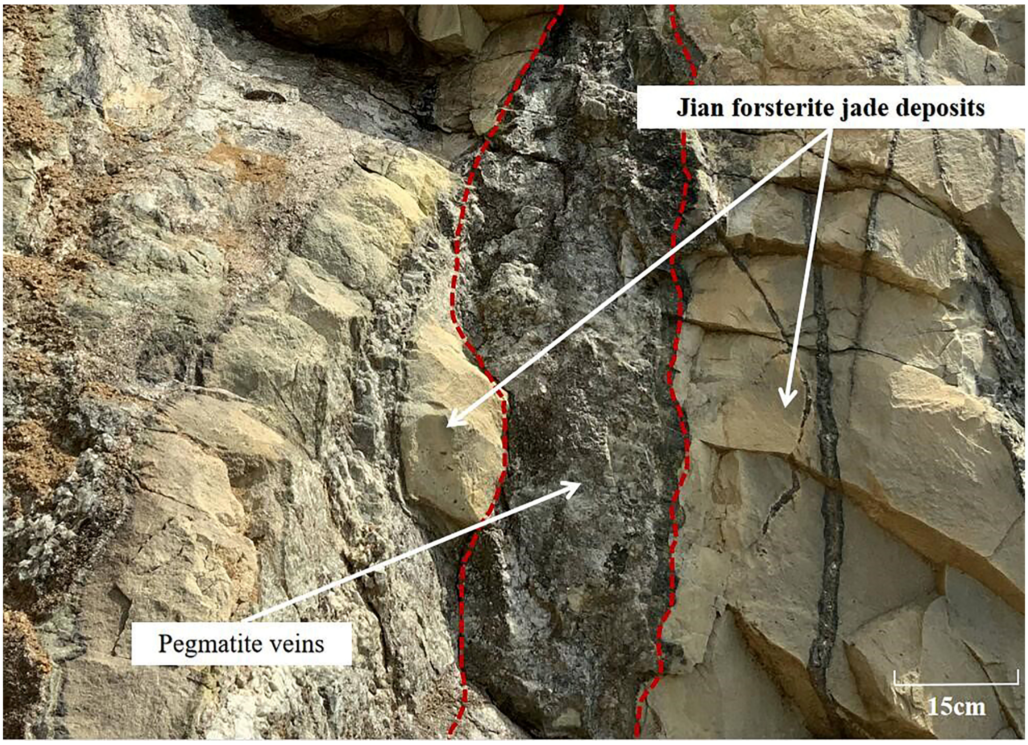

Figure 3. Pegmatite veins interspersed in Jian forsterite jade deposits.

3. Materials and Methods

3.1. Materials

The samples for this study were collected from the Jian forsterite jade deposits, located at 125°39′ E, 41°20′18′′ N, at an altitude of 460 m. Based on the geological characteristics of the field, the collected samples were compiled, and six representative samples were selected for the study, which can be divided into three main types (Table 1) (Figure 4). Type 1 is tourmaline from the core (D15-2) and the side (JAG18) of the pegmatite veins. Type 2 is tourmaline from the distal jade end (D05-2) and the near-jade end (JA23, JA24) in the contact zone between the pegmatite veins and the Jian forsterite jade. Type 3 is tourmaline from the tourmaline veins in the Jian forsterite jade (JAD06).

Table 1. Samples of magnesium tourmalines and their characteristics.

Types	Sample No.	Formation Position	Characteristics
Type 1	D15-2 JAG18	Core of the pegmatite veins Side of the pegmatite veins	black-brown, a patchy distribution, coeval with quartz, albite, orthoclase, magnesium biotite, titanite, and actinolite.
Type 2	D05-2	Distal jade end in the zone	yellow-brown, aggregated in clumps or short columns, coeval with oligoclase, phlogopite, tremolite, apatite, and zircon.
	JA23 JA24	Near-jade end in the zone	
Type 3	JAD06	Tourmaline veins in jade	yellow-brown, coeval with phlogopite and tremolite.

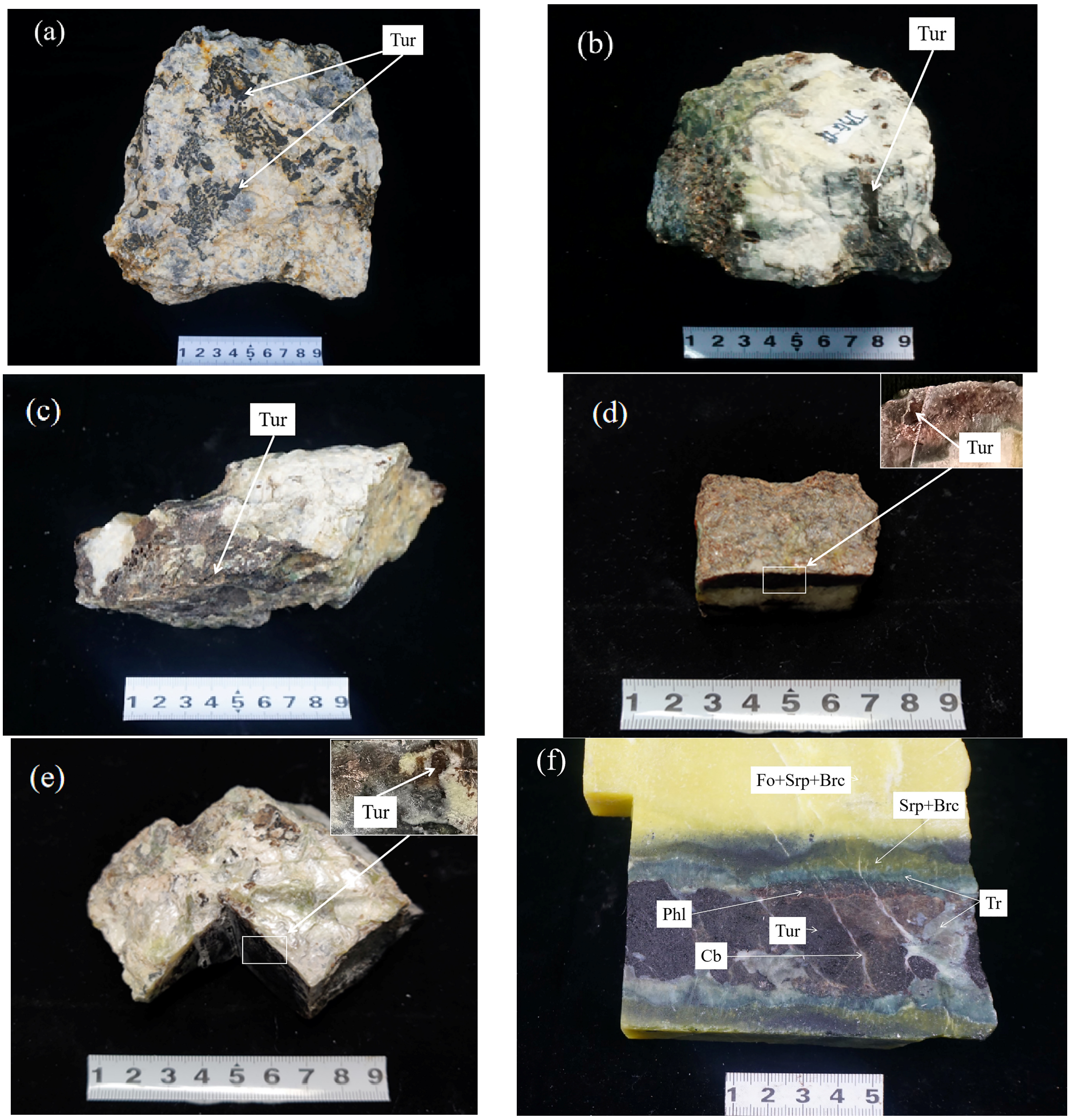

Figure 4. (**a**) Tourmaline in the core of pegmatite veins (D15-2); (**b**) Tourmaline in the side of pegmatite veins (JAG18); (**c**) Tourmaline from the distal jade end (D05-2); (**d**) Tourmaline from the near-jade end (JA23); (**e**) Tourmaline from the near-jade end (JA24); (**f**) Tourmaline from tourmaline veins in Jian forsterite jade (JAD06). Tur, tourmaline; Or, orthoclase; Bt, biotite; Tr, tremolite; Phl, phlogopite; Cb, carbonate minerals; Fo, forsterite; Srp, serpentine; Brc, brucite.

3.2. Methods

3.2.1. Electron Microprobe Analysis

Electron probe microanalysis (EPMA) is an increasingly important analysis tool in materials science and geosciences [34]. This test was performed at the Institute of Mineral Resources at the Chinese Academy of Geological Sciences (CAGS) using a JXA-iHP200F electronic probe equipped with 5 wavelength-dispersive spectrometers (JEOL, Tokyo, Japan). The samples were plated with a carbon film of about 20 nm thickness as uniformly as possible before being tested on the machine. The test working conditions were an accelerating voltage of 15 kV, an accelerating current of 20 nA, and a beam spot diameter of 5 μm. Natural minerals and synthetic oxides were used as standards. The data were corrected online using a modified ZAF (atomic number, absorption, fluorescence) correction procedure.

3.2.2. Micro-XRF Mapping Analysis

The test was performed in the laboratory of the National Infrastructure of Mineral, Rock and Fossil Resources for Science and Technology (NIMRF). The experimental instrument was a micro-area X-ray fluorescence spectrometer (M4 Tornado model) manufactured by Bruker (Ettlingen, Germany). The range of elemental analysis was Na~U, voltage 50 KV, current 599 μA, scan time 10 ms/pixel, pixel size 20 μm, and total test time 14 h.

3.2.3. Laser Ablation-ICP-MS Analysis

The test was performed at the National Geological Experimental Testing Center, China Geological Survey (CGS). The laser used for the LA-ICP-MS experiments was a yttrium aluminum garnet system from New Wave, USA, with a wavelength of 213 nm, and the mass spectrometer was a Thermo Element II from Finnigan, Germany. The instrument was adjusted for laser exfoliation at a beam spot diameter of 45 μm, a frequency of 10 Hz, and an energy density of approximately 9 J/cm^2 to obtain 232 Th by line scan exfoliation of NIST SRM 612 with an oxide yield of ThO/Th < 0.3%. The samples were sampled by single-point exfoliation in the mode of 20 s gas blank +40 s sample exfoliation +20 s rinse, with a set of specimens inserted at every 20 unknown sample points. Each sample was tested for more than 50 isotopes, including 7Li~238U at the same time, and each isotope was tested for 4 ms with peak-hopping acquisition. NIST SRM 612 and KL2-G were used as external standards for the data correction, and the data processing was performed using the matrix normalization method with 29Si as the internal standard.

4. Results

4.1. Petrography

In type 1 tourmaline, the color is brownish-black. Tourmaline and quartz, albite, orthoclase, and other mineral associations are developed in the core of the pegmatite veins, while tourmaline and magnesium biotite, tanzanite, actinolite, and other mineral associations are developed in the sides of the pegmatite veins (Figure 5a–f). In type 2 tourmaline, the color is yellowish-brown and develops mineral associations of tourmaline with oligoclase, phlogopite, tremolite, apatite, and zircon (Figure 5g–i). In type 3 tourmaline, the color is yellowish-brown and develops mineral associations of tourmaline with phlogopite, tremolite, forsterite, serpentine, brucite, and carbonate minerals (Figure 5j,k).

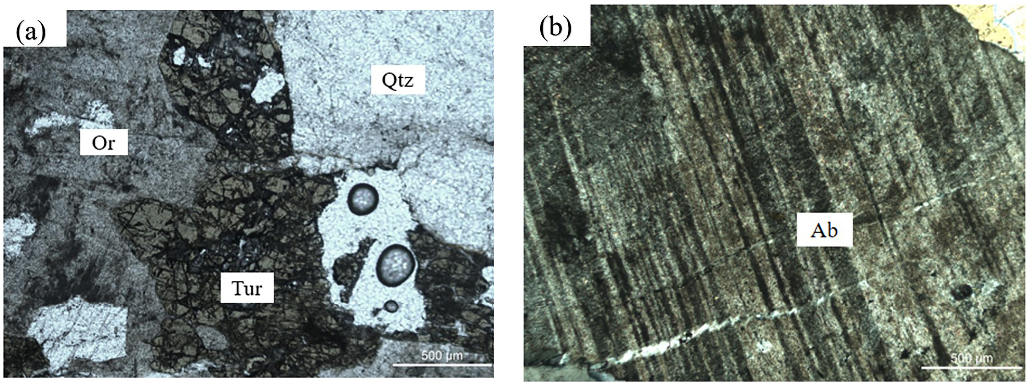

Figure 5. *Cont.*

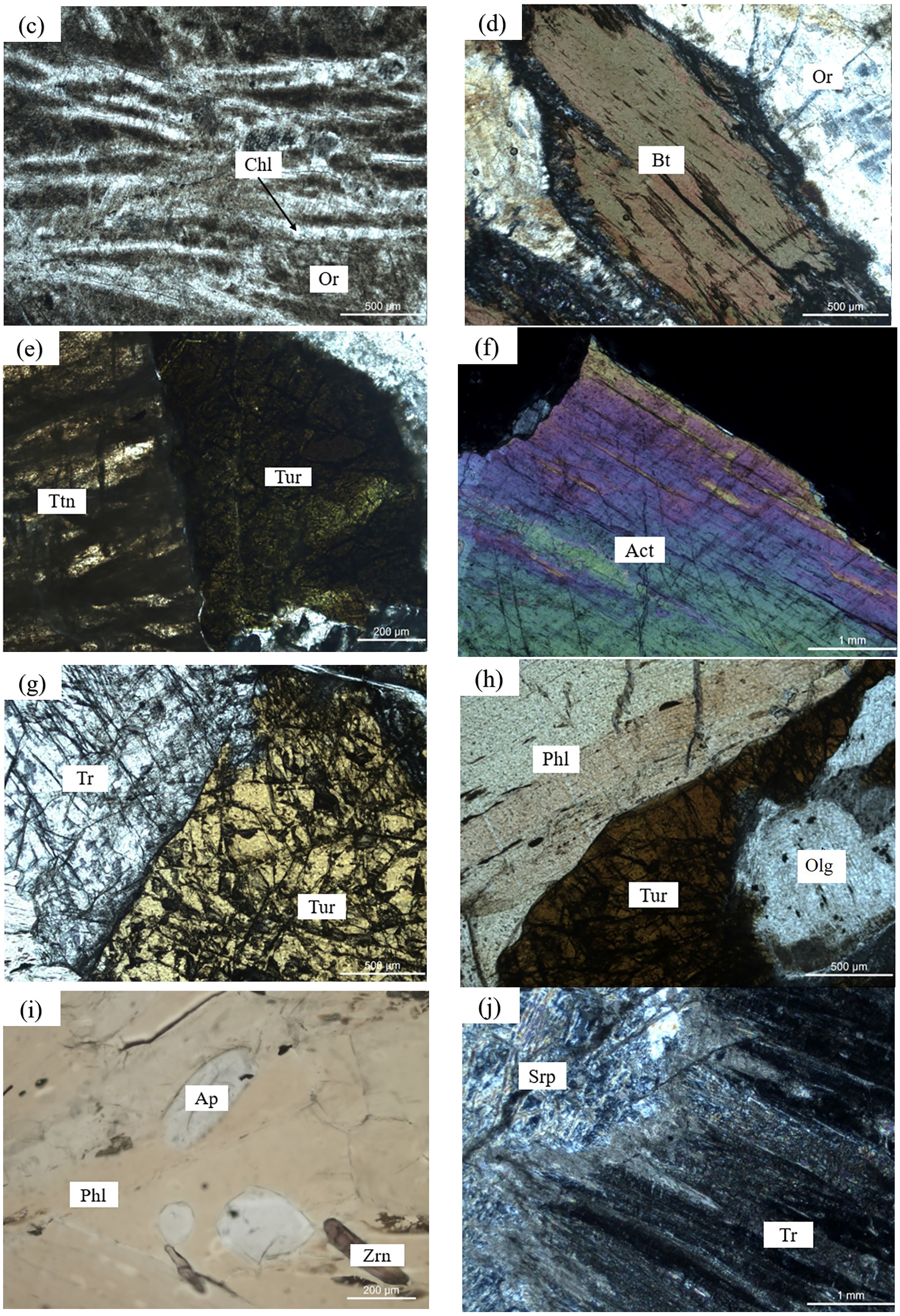

Figure 5. *Cont*.

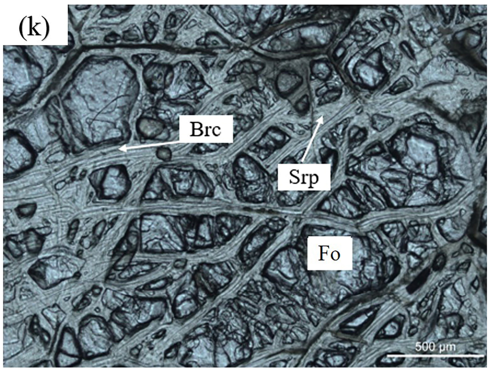

Figure 5. (**a**) The relationship between tourmaline and quartz and orthoclase; (**b**) Albite developed with polysynthetic twin; (**c**) Chloritization occurs in orthoclase; (**d**) The relationship between magnesium biotite and orthoclase; (**e**) The relationship between tourmaline and titanite; (**f**) Large grains of actinolite appear as secondary interference colors; (**g**) The relationship between tourmaline and tremolite; (**h**) The relationship between tourmaline, oligoclase, and phlogopite; (**i**) The relationship between phlogopite, apatite, and zircon; (**j**) The relationship between tremolite and serpentine; (**k**) The relationship between forsterite, serpentine, and brucite. Tur, tourmaline; Qtz, quartz; Or, orthoclase; Ab, albite; Bt, biotite; Chl, chlorite; Tth, tiantite; Act, actinolite; Tr, tremolite; Olg, oligoclase; Phl, phlogopite; Ap, apatite; Zrn, zircon; Cb, carbonate minerals; Fo, forsterite; Srp, serpentine; Brc, brucite.

4.2. Major Element Compositions

Tourmaline has a complex chemical composition, and its general formula is generally represented as $XY_3Z_6[T_6O_{18}][BO_3]_3V_3W$, where X = Na^+, Ca^{2+}, K^+, □(X-vacancy); Y = Fe^{2+}, Mg^{2+}, Mn^{2+}, Al^{3+}, Li^+, Fe^{3+}, Ti^{4+}, V^{3+}, Cr^{3+}; Z = Al^{3+}, Fe^{3+}, Mg^{2+}, Cr^{3+}, V^{3+}; T = Si^{4+}, Al^{3+}, B^{3+}; B = B^{3+}; and V = OH^-, O^{2-}; W = OH^-, F^-, O^{2-} [35–40]. In this paper, the calculation is normalized based on the sum of the number of cations at positions Y, Z, and T equal to 15 (Y + Z + T = 15). Since the electronic probe cannot detect the content of B_2O_3 and H_2O, the calculation is performed assuming the unit atomic number B = 3 and OH + F + Cl = 4. Because the electron probe could not distinguish between Fe^{2+} and Fe^{3+}, all the Fe was assumed to be Fe^{2+}.

The major element compositions of type 1, type 2, and type 3 tourmaline are shown in Table S1. The tourmalines in the Jian forsterite jade deposits contained SiO_2 (35.32~40.09 wt. %), Al_2O_3 (25.53~31.08 wt. %), TiO_2 (0.25~2.72 wt. %), FeO (0.94~11.17 wt. %), MgO (7.15~14.39 wt. %), Na_2O (0.62~2.15 wt. %), and CaO (1.33~4.36 wt. %), and the compositions of the three types of tourmalines were significantly different.

The tourmalines in Jian forsterite jade deposits include two major groups: the calcic group and the alkali group, as well as uvite and dravite. They are both magnesium tourmaline. The type 1 tourmaline (D15-2, JAG18) is alkali tourmaline and dravite. The distal jade end (D05-2) of type 2 tourmaline is alkali tourmaline and dravite, and the near-jade end (JA23, JA24) is calcic tourmaline and uvite. Type 3 tourmaline includes both the alkali group (central) and the calcic group (side) and also includes both dravite (central) and uvite (side) (Figure 6a,b).

In the Al–Fe–Mg diagram, the type 1 tourmaline plots in the region of Fe^{3+}-rich quartz–tourmaline rocks, calc–silicate rocks, and metapelites, and the type 2 and 3 tourmalines plot in the region of metacarbonates and metapyroxenites (Figure 6c). In the Ca–Fe–Mg diagram, the type 1 tourmaline and the distal jade end of the type 2 tourmaline plots in the area of Ca-poor metapelites, metapsammites, and quartz–tourmaline rocks, and the near-jade end of the type 2 tourmaline falls into the area of metacarbonates, while the type 3 tourmaline is distributed in both of these areas (Figure 6d).

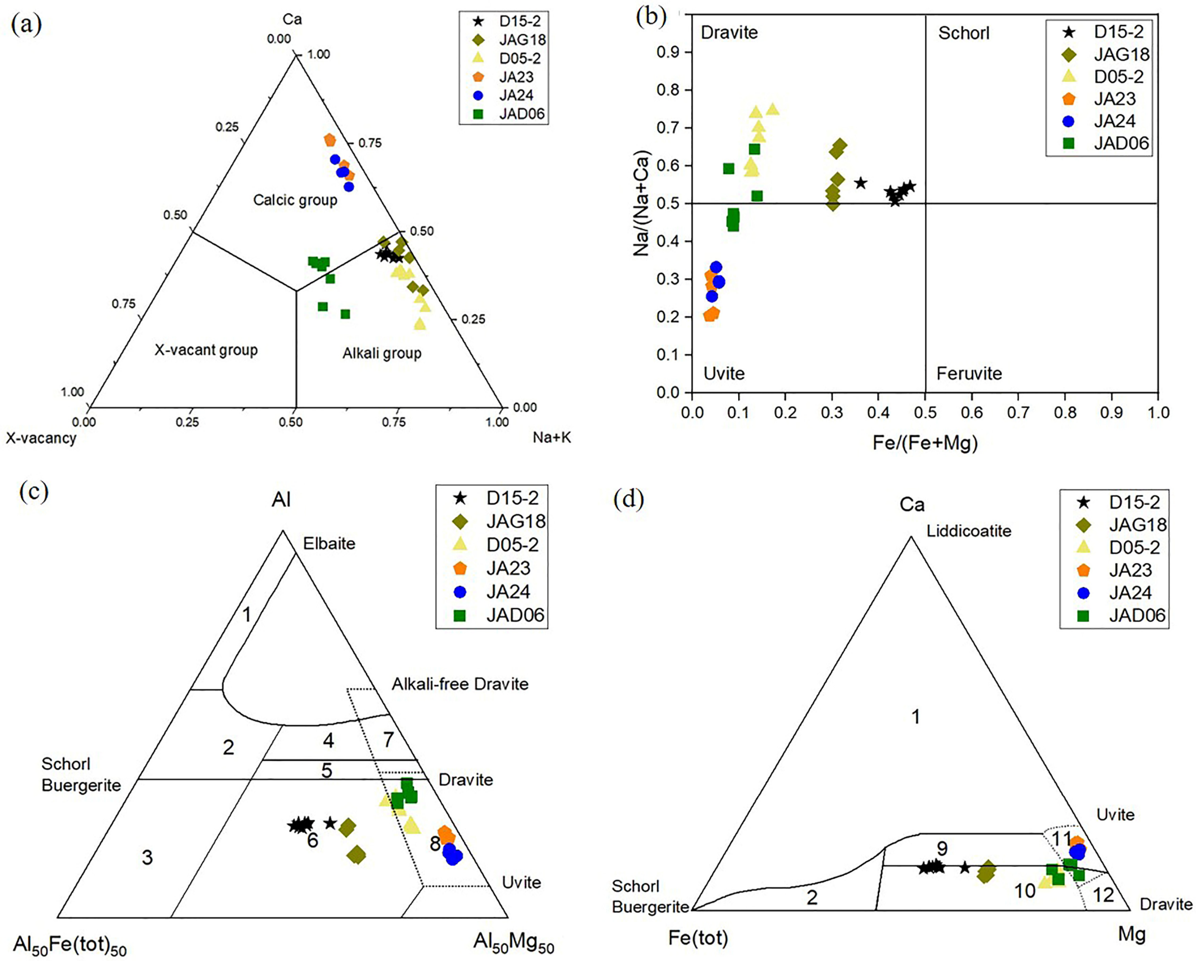

Figure 6. (**a**) Classification of the principal groups of tourmaline based on X-site occupancy [37]. (**b**) Nomenclature of the tourmaline based on the classification diagram of Fe/(Fe + Mg) versus Na/(Na + Ca) [41]. (**c**,**d**) Ternary Al–Fe–Mg and Ca–Fe–Mg diagrams showing compositions of tourmaline [10]. The regions define the compositions of tourmalines from different rock types. 1. Li-rich granitoids and associated pegmatites and aplites; 2. Li-poor granitoids and associated pegmatites and aplites; 3. Fe^{3+}-rich quartz–tourmaline rocks (hydrothermally altered granites); 4. Metapelites and metapsammites coexisting with an Al-saturating phase; 5. Metapelites and metapsammites not coexisting with an Al-saturating phase; 6. Fe^{3+}-rich quartz–tourmaline rocks, calc silicate rocks, and metapelites; 7. Low-Ca metaultramafics and Cr, V-rich metasediments; 8. Metacarbonates and metapyroxenites; 9. Ca-rich metapelites, metapsammites, and calc-silicate rocks; 10. Ca-poor metapelites, metapsammites, and quartz-tourmaline rocks; 11. Metacarbonates; 12. Metaultramafics.

Tourmaline in areas of hydrothermal accounting with enclosing rocks or in intrusive pegmatite veins may not be well summarized because the composition of tourmaline is partially or fully influenced by the chemistry of the enclosing rocks, but it can provide some information about the nature of the original rocks [10]. In general, type 1 tourmaline has an affinity with Fe^{3+}-rich quartz–tourmaline rocks and low-Ca metasediments, while type 2 and 3 tourmalines have an affinity with metacarbonates.

The binary diagrams show the variation in the major elements in type 1, 2, and 3 tourmaline samples (Figure 7). The substitution of $Fe^{2+}{}_{-1}Mg^{2+}{}_{-1}$ is evident in the plots of Mg (apfu) versus Fe^{tot} (apfu). The substitution of $(\square Al^{3+})_{-1}(Na^{+}Mg^{2+})_{-1}$ is visible in the plots of Mg (apfu) versus Ca (apfu). The substitution of $(\square Al^{3+}{}_{2})_{-1}(Ca^{2+}R^{2+}{}_{2})_{-1}$ is visible in the diagrams of Al (apfu) versus X-vacancy (apfu). The substitutions of $(Ca^{2+}Mg^{2+})_{-1}(Na^{+}Al^{3+})_{-1}$ or $(Ca^{2+}O^{2-})_{-1}(Na^{+}OH^{-})_{-1}$ are visible in the diagrams of Ca (apfu) versus Na (apfu).

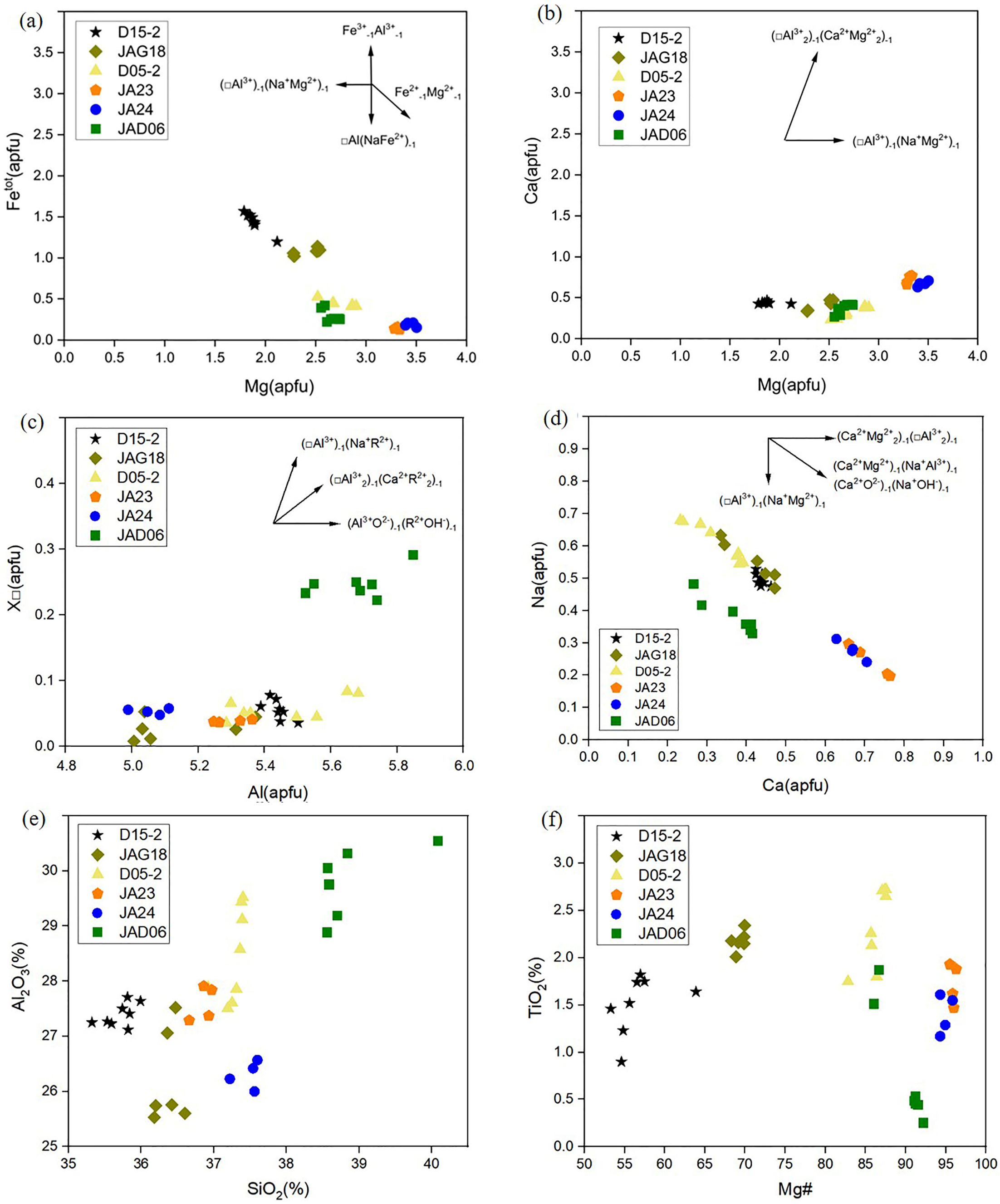

Figure 7. Binary diagrams of major element compositions of magnesium tourmaline. (**a**) Mg (apfu) versus Fe^{tot} (apfu); (**b**) Mg (apfu) versus Ca (apfu); (**c**) Al (apfu) versus X-vacancy (apfu); (**d**) Ca (apfu) versus Na (apfu); (**e**) SiO_2 (wt.%) versus Al_2O_3 (wt.%); (**f**) Mg# versus TiO_2 (wt.%).

4.3. Major Element Distribution (XRF Mapping)

The tourmaline sample (type 3 tourmaline) in the tourmaline veins of Jian forsterite jade is rich in tourmaline and other mineral associations, and the minerals between tourmaline and jade have obvious zoning characteristics, which is a typical sample for studying the spatial relationship and formation process of tourmaline and Jian forsterite, so this sample was selected for the Micro-XRF Mapping test. The XRF Mapping signal intensity distribution characteristics of the 10 major elements, such as Si, Al, Fe, Mg, Ti, V, K, Na, Ca, and Mn, of tourmaline and tremolite, phlogopite, serpentine, forsterite, and other minerals were measured, and the elemental concentration steps from high to low showed the colors of red, orange, yellow, green, blue, purple, and black in order (Figure 8).

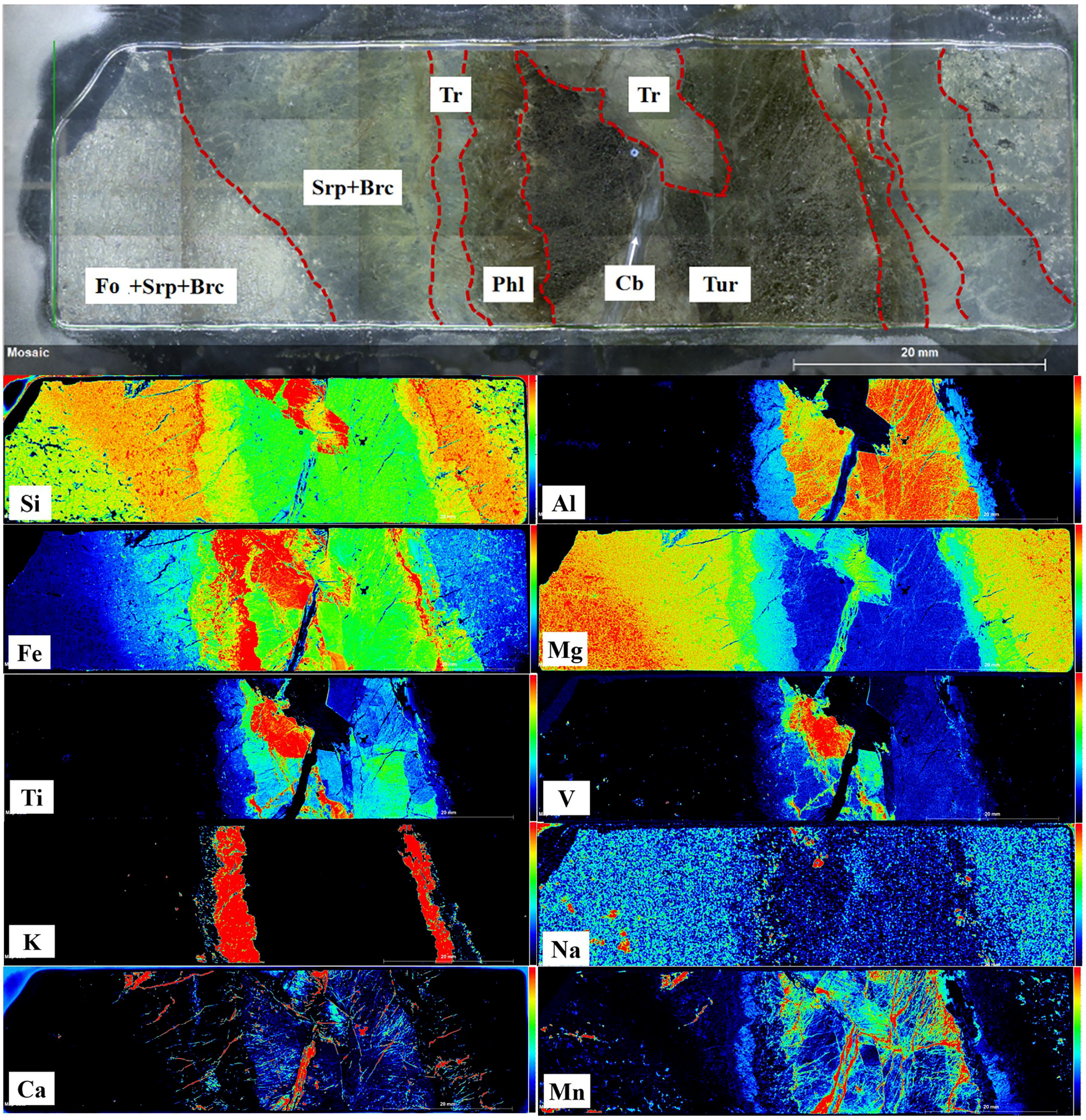

Figure 8. Major element (Si, Al, Fe, Mg, Ti, V, K, Na, Ca, and Mn) distribution of type 3 tourmaline. Tur, tourmaline; Tr, tremolite; Phl, phlogopite; Cb, carbonate minerals; Fo, forsterite; Srp, serpentine; Brc, brucite.

The minerals with high to low Si content are tremolite, serpentine, phlogopite, Jian forsterite jade (mainly forsterite + serpentine + brucite), and tourmaline, and the minerals with high to low Al content are tourmaline, phlogopite, and tremolite. The concentrations of Fe and Mg elements generally show opposite trends, with Jian forsterite jade having the highest Mg element content, followed by serpentine, tremolite, muscovite, and tourmaline. The concentration of Na is not high in the sample overall but is slightly higher in the Jian forsterite jade than in the tourmaline veins, and the contents of Ca and Mn show similar distribution characteristics, roughly along the small fractures in the mineral.

In general, Si, Al, Fe, and Mg in tourmaline are well distributed and vary regularly with co-associated minerals, Ti, V, and some Fe are locally uneven, and Ca and Mn are enriched along the fractures.

4.4. Trace and Rare Earth Element Compositions

The trace and rare earth element (REE) compositions of magnesium tourmaline are sensitive indicators of the petrogenic environment and infer hydrothermal origin, composition, and evolution (Table S2). The porphyritic granites of Paleoproterozoic granitoids in the Liao–Ji region have S-type peraluminous granite-style features with obvious light and heavy rare earth element differentiation, high LREE/HREE [28]. The magnesium tourmaline in Jian forsterite jade deposits has a similar REE pattern to the Liaoji porphyritic granite, suggesting that the mineralizing fluid may have come from its post-period hydrothermal origin.

The REE patterns of the three types of tourmalines are generally similar and have typical LREE enrichment relative to HREE with obvious positive Eu anomalies, reflecting the close relationship between mineralization and host rocks and the strong environmental control of tourmaline [42] (Figure 9a). The REE characteristics of tourmaline are controlled by crystal chemistry, and tourmaline tends to incorporate Eu^{2+} into the X position in the lattice more than Eu^{3+}. Therefore, the rare earth element characteristics of tourmaline may reflect the dominant presence of Eu^{2+} in the mineralized hydrothermal fluid [43].

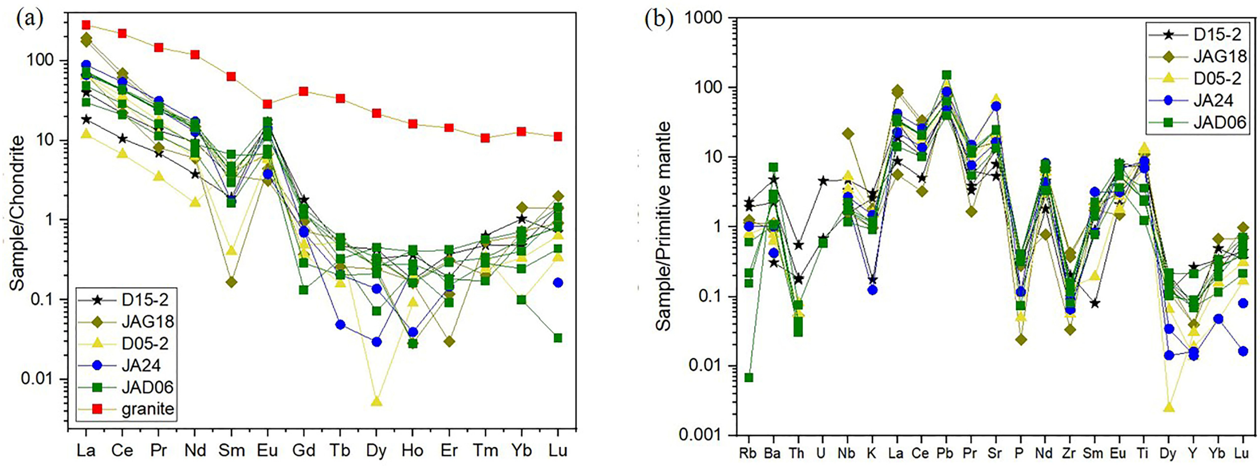

Figure 9. (**a**) Chondrite-normalized [42] REE patterns of magnesium tourmaline in Jian forsterite jade deposits. Note that the chondrite-normalized REE patterns of Liaoji porphyritic granite [28] are also shown for comparison. (**b**) Primitive mantle-normalized [44] spider diagram of magnesium tourmalines in Jian forsterite jade deposits.

The primitive mantle-normalized spider diagrams of the three types of tourmalines are generally similar in appearance [44] (Figure 9b). Among the high field strength elements (HFSE), tourmaline is relatively deficient in elements such as Th, P, and Zr, which may be related to the fact that during mineral formation, these elements tend to be more enriched in minerals such as zircon, apatite, and titanite and less allocated to tourmaline. The ions of Pb elements have two forms, Pb^{2+} or Pb^{4+}, and, usually, Pb^{4+} is considered a high field strength element, while Pb^{2+} is a large ion-lithophile element, and it has been shown that Pb elements in tourmaline are usually present as Pb^{2+} at the X-site in the lattice [45,46]. Among the large ion-lithophile elements (LILE), tourmaline is relatively enriched in Pb^{2+}, Sr, and Eu^{2+}, indicating that tourmaline is the main fugitive mineral for large ion-lithophile elements. The relative deficit of K elements in tourmaline may be because, during mineral formation, K elements tend to be more enriched in mica group minerals and, thus, are present in tourmaline in small amounts.

The binary diagram between the Zn, K, Mn, Sc, Ga, and Co elements of tourmaline is shown in Figure 10. The Zn content of magnesium tourmaline in Jian forsterite jade deposits ranges from 8.80 to 126.80 ppm, the K content from 0 to 737.56 ppm, the Mn content from 7.52 to 422.78 ppm, the Sc content from 2.38 to 48.46 ppm, the Ga content from 25.02 to 71.27 ppm, the Co content from 1.06 to 15.31 ppm, the Sr content from 106.35~1342.37 ppm, and the Sn content from 8.81 to 94.64 ppm.

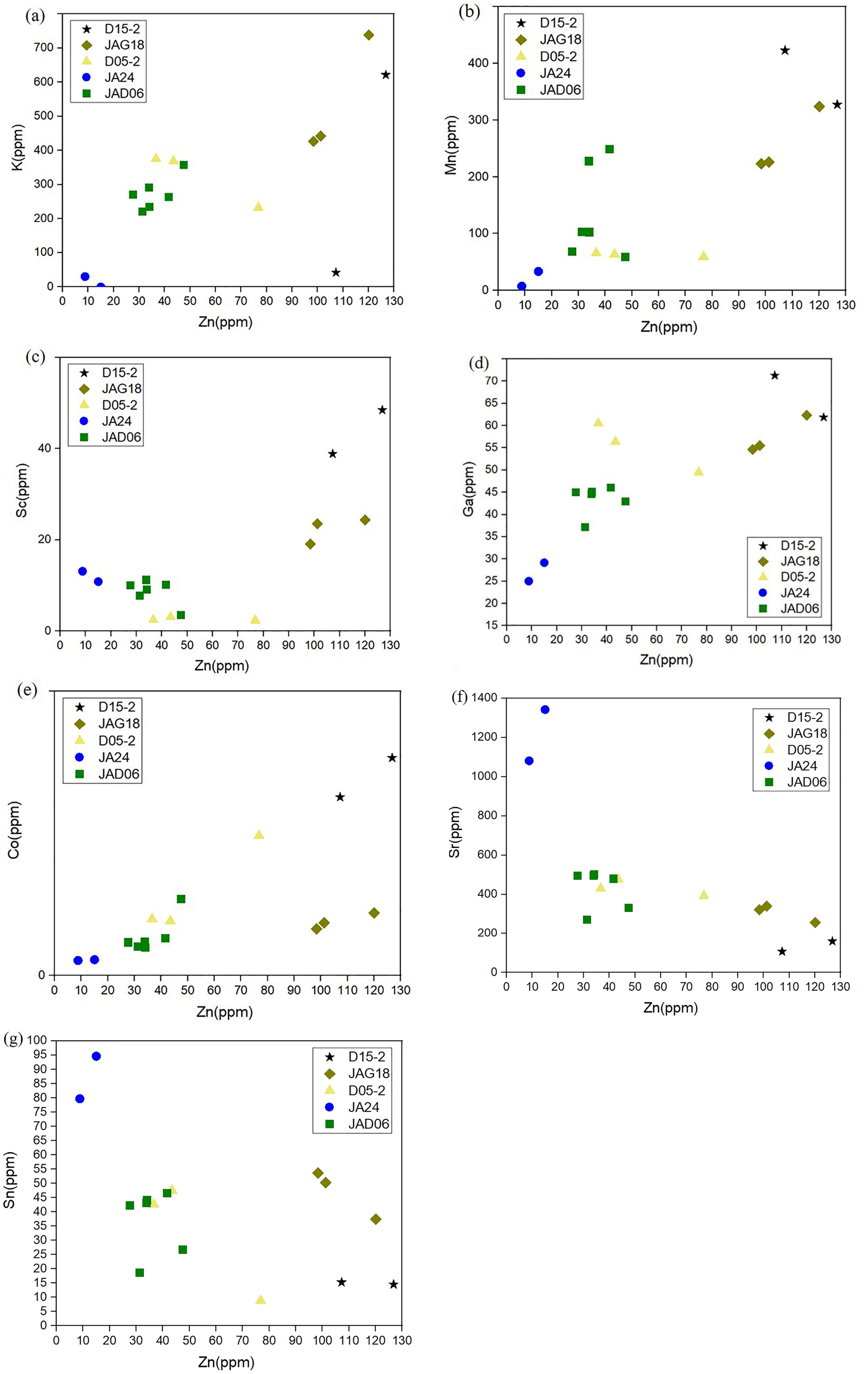

Figure 10. Binary diagrams of trace element compositions of magnesium tourmaline (ppm). (**a**) Zn versus K; (**b**) Zn versus Mn; (**c**) Zn versus Sc; (**d**) Zn versus Ga; (**e**) Zn versus Co; (**f**) Zn versus Sr; (**g**) Zn versus Sn.

5. Discussion

5.1. Genesis of Magnesium Tourmaline

Depending on the type of genesis, tourmaline can be mainly classified as magmatic, hydrothermal, and metamorphic [15–20]. Tourmaline of magmatic genesis is usually not seen under the microscope as distinct color zoning and is characterized by high Fe/Mg ratios with higher Al in the Y position of the tourmaline lattice and a lower content of V and Sr. Tourmaline of hydrothermal genesis usually appears to have more complex growth rings and usually has a lower Li and higher V and Sr content in the chemical composition [10,19,20,47]. Metamorphic diagenesis refers to the formation of tourmaline after metamorphism in different petrographic phases, such as metagranite, sepiolite, and hornblende [48]. The petrographic observations of magnesium tourmaline in Jian forsterite jade deposits did not reveal any obvious growth rings, but local color differences were observed in some of the tourmaline grains. The EPMA tests showed that the three different types of tourmaline samples are characterized as Mg-rich (Mg# = 53.27~96.28), falling into the Mg tourmaline or Ca–Mg tourmaline region, with a lower Al content (4.989~5.849 apfu) at the tourmaline Y position. The LA-ICP-MS tests showed that tourmaline has a lower Li (9.07~54.66 ppm)d, a higher V (36.41~268.53 ppm) and Sr (106.35~1342.17 ppm) content. The results of this article are in agreement with most of the hydrothermal genesis tourmaline.

The tourmaline forms in areas close to pegmatites are brownish-black and coeval with quartz, albite orthoclase, biotite, titanite, and actinolite (type 1). The tourmaline formed in the contact zone is yellowish-brown in color and coeval with oligoclase, phlogopite, tremolite, apatite, and zircon (type 2). The tourmaline from tourmaline veins in the jade shows high concentrations of Si and Al, and the rest of the chemical composition is roughly between the above two types, and the large tourmaline grains may be related to its enrichment and rapid crystallization in Si- and Al-rich mineralizing hydrothermal fluids (type 3). After the formation of tourmaline, the later Mn- and Ca-bearing secondary minerals filled and crystallized in the fractures.

In general, between tourmaline and Jian forsterite jade, there are phlogopite, tremolite, and serpentine bands, and the fractures of some tourmaline are filled with secondary carbonate minerals (Figure 4f). Based on the above experiments, it is assumed that the formation and evolution of tourmaline are based on the intrusion of pegmatite-related hydrothermal fluids into Jian forsterite jade, the strong contact metasomatic metamorphism between them due to the difference in physicochemical properties, and the formation of various co-associated mineral assemblages in the process. The pegmatite-related hydrothermal fluids provide abundant Si, Al, Fe, Na, K, and some Ca elements for the formation of tourmaline, and Jian forsterite jade provides mainly Mg and some Ca elements.

5.2. Constraints on Variation of the Chemical Composition of Magnesium Tourmaline

The analysis of the major elemental composition of magnesium tourmaline shows that the content of Si and Mg gradually increases and the content of the Fe element gradually decreases from the type 1 tourmaline (the core to the side of the vein) to the type 2 tourmaline (the distal jade end to the near-jade end) (Figure 7e,f). In addition, the variation in the Ca and Na content of tourmaline shows certain special characteristics. From the type 1 tourmaline to the type 2 tourmaline, the overall Ca content gradually decreases while the Na element gradually increases, and from the distal jade end to the near-jade end of the type 2 tourmaline, the Ca content gradually increases while the Na gradually decreases. The content of Si and Al in the type 3 tourmaline is significantly higher than those two types of samples; the content of Fe, Mg, Ca, and Na is generally in between the above two types.

In terms of the trace elements, the elements of Zn, K, Mn, Sc, Ga, and Co gradually decrease, Sr and Sn gradually increase from the type 1 tourmaline (the core to the side of the vein) to the type 2 tourmaline (the distal jade end to the near-jade end), and the content of Zn, K, Mn, Sc, Ga, Co, Sr, and Sn of the type 3 tourmaline generally lies between the above two types (Figure 10).

The pattern of change in the composition of the magnesium tourmaline's major and trace elements suggests that its formation is strongly constrained by the enclosing rock (Jian forsterite jade). The tourmaline formed closer to the Jian forsterite jade has a higher Mg content and is complemented by Ca (type 1), while closer to the pegmatite veins, the tourmaline has a higher Fe content and Na dominates in the X position (type 2). The tourmaline in the tourmaline veins (type 3) is at a distance from the Jian forsterite jade between type 1 and type 2 tourmaline, so the Mg, Fe, etc. content is also between them.

5.3. Implications for Jian Forsterite Jade Formation and Evolution

The mechanism of the Jian forsterite jade is not well understood. It may be formed by fluid serpentinization of the ancient refractory lithospheric mantle of the North China Craton by a possible subduction plate dehydration process or by contact metamorphism between silica-rich fluids and Mg-rich dolomite [2,3]. A study of the chemical composition of the three types of tourmaline revealed that the closer the tourmaline formed to the Jian forsterite jade, the more Mg-rich it was, in addition to some Ca supplementation (Table S1) (Figure 7a,d). The host rock environment is related to the metacarbonates (Figure 6c,d). This may indicate that the genesis of Jian forsterite jade is more inclined to the contact metamorphism of siliceous fluids and Mg-rich dolomite proposed by Peng et al. [3].

The main constituent minerals of Jian forsterite jade are forsterite, serpentine, and brucite, and the degree of serpentinization can vary. According to the field geological characteristics and tourmaline co-associated mineral assemblage, it has been found that the contact zone between hydrothermal fluid and the surrounding rocks, where tourmaline is formed, often forms a tremolite zone first and the degree of serpentinization is stronger, and different degrees of serpentinization also show obvious zoning phenomenon (Figure 4f). Therefore, it is believed that the pegmatite-related hydrothermal fluids reacted with the Jian forsterite jade, which probably contained calcium carbonate minerals. As the contact metasomatic metamorphism proceeded, minerals such as tremolite, phlogopite, and tourmaline were formed, and further serpentinization occurred in the jade [49,50] (Equation (1)).

$$\underset{\text{Serpentine}}{5Mg_3Si_2O_5(OH)_4} + 14SiO_2(aq) + 6CaO = \underset{\text{Tremolite}}{3Ca_2Mg_5Si_8O_{22}(OH)_2} + 7H_2O \tag{1}$$

At the same time, the texture and transparency of the Jian forsterite jade are enhanced as the serpentinization proceeds. Therefore, the chemical composition of the three types of tourmalines studied in this paper indicates the fluid characteristics of the gradual serpentinization of Jian forsterite, which is indicative of its formation and evolution.

6. Conclusions

1. Three types of tourmalines are recognized in Jian forsterite jade deposits. They are both magnesium tourmalines and include two major groups: the calcic group and the alkali group, as well as uvite and dravite.
2. The substitutions of $Fe^{2+}{}_{-1}Mg^{2+}{}_{-1}$, $(\square Al^{3+})_{-1}(Na^{+}Mg^{2+})_{-1}$, $(\square Al^{3+}{}_2)_{-1}(Ca^{2+}R^{2+}{}_2)_{-1}$, $(Ca^{2+}Mg^{2+})_{-1}(Na^{+}Al^{3+})_{-1}$, and $(Ca^{2+}O^{2-})_{-1}(Na^{+}OH^{-})_{-1}$ are inferred by the variations in the major element compositions of magnesium tourmaline.
3. From type 1 to type 2 tourmaline, the content of Mg, Sr, and Sn gradually increases, the content of Fe, Zn, K, Mn, Sc, Ga, and Co gradually decreases, the content of Ca initially decreases and then increases, and the content of Na first increases and then decreases. Type 3 tourmaline has significantly higher Si and Al than the first two types, and the content of the remaining elements lies between the above two types.
4. Tourmalines are typically of hydrothermal origin and are mainly constrained by magnesium, which is a pegmatite-related hydrothermal fluid and Jian forsterite jade with contact metasomatic metamorphism, in which hydrothermal fluid provides Si,

Al, Fe, Na, K, and some Ca elements, and Jian forsterite jade provides Mg and some Ca elements.

5. The chemical composition of tourmaline indicates the fluid characteristics of the gradual serpentinization of Jian forsterite jade.

Supplementary Materials: The following supporting information can be downloaded at: https://www.mdpi.com/article/10.3390/cryst13121653/s1, Table S1: Major element compositions of type 1, type 2 and type 3 tourmaline samples in Jian forsterite jade deposits, Table S2: Trace element compositions of tourmaline samples in Jian forsterite jade deposits.

Author Contributions: Conceptualization, M.H.; methodology, M.H. and M.Y.; software, H.Y.; formal analysis, H.Y.; investigation, H.Y., B.P., S.W. and Y.S.; resources, M.H. and M.Y.; data curation, H.Y. and S.W.; writing—original draft preparation, H.Y.; writing—review and editing, H.Y., M.H. and B.P.; supervision, M.H. and M.Y.; funding acquisition, M.H. and M.Y. All authors have read and agreed to the published version of the manuscript.

Funding: National Mineral Rock and Fossil Specimens Resource Center.

Data Availability Statement: Data is contained within the article or Supplementary Materials.

Acknowledgments: We thank Haiyang Yu and Yingliang Jiang from Ji'an Xinli Mining Co., Ltd. for the field investigation. We are grateful to the editors and anonymous reviewers whose comments improved the quality of the manuscript.

Conflicts of Interest: The authors declare no conflict of interest.

References

1. Han, W.; Chen, H.; Ke, J.; Lu, T. Characterization of "Ganlan" Jade and Nomenclature. In Proceedings of the Gemology & Technology-2015 China Gems & Jewelry Academic Conference, Beijing, China, 30 November 2015.
2. Wang, Y.; He, M.; Yan, W.; Yang, M.; Liu, X. Jianite: Massive Dunite Solely Made of Virtually Pure Forsterite from Ji'an County, Jilin Province, Northeast China. *Minerals* **2020**, *10*, 220. [CrossRef]
3. Peng, B.; He, M.; Yang, M.; Liu, X.; Sui, X.; Sun, K.; Wu, S. Petrogenesis of Jian forsterite jade solely composed of end-member forsterite (Fo 99.8): Constrained by trace element and oxygen isotope. *Ore Geol. Rev.* **2022**, *150*, 105167. [CrossRef]
4. Xu, B.; Griffin, W.L.; Xiong, Q.; Hou, Z.-Q.; O'reilly, S.Y.; Guo, Z.; Pearson, N.J.; Gréau, Y.; Yang, Z.-M.; Zheng, Y.-C. Ultrapotassic rocks and xenoliths from South Tibet: Contrasting styles of interaction between lithospheric mantle and asthenosphere during continental collision. *Geology* **2017**, *45*, 51–54. [CrossRef]
5. Sobolev, N.V.; Logvinova, A.M.; Zedgenizov, D.A.; Pokhilenko, N.P.; Malygina, E.V.; Kuzmin, D.V.; Sobolev, A.V. Petrogenetic significance of minor elements in olivines from diamonds and peridotite xenoliths from kimberlites of Yakutia. *Lithos* **2009**, *112*, 701–713. [CrossRef]
6. Wilson, A.; Bolhar, R. Olivine in komatiite records origin and travel from the deep upper mantle. *Geology* **2022**, *50*, 351–355. [CrossRef]
7. Vance, J.A.; Dungan, M.A. Formation of peridotites by deserpentinization in the Darrington and Sultan areas, Cascade Mountains, Washington. *Geol. Soc. Am. Bull.* **1977**, *88*, 1497–1508. [CrossRef]
8. Xiong, F.; Yang, J.; Robinson, P.T.; Xu, X.; Liu, Z.; Li, Y.; Li, J.; Chen, S. Origin of podiform chromitite, a new model based on the Luobusa ophiolite, Tibet. *Gondwana Res.* **2015**, *27*, 525–542. [CrossRef]
9. Nekrylov, N.; Plechov, P.Y.; Gritsenko, Y.D.; Portnyagin, M.V.; Shcherbakov, V.D.; Aydov, V.A.; Garbe-Schönberg, D. Major and trace element composition of olivine from magnesian skarns and silicate marbles. *Am. Mineral.* **2021**, *106*, 206–215. [CrossRef]
10. Henry, D.J.; Guidotti, C.V. Tourmaline as a petrogenetic indicator mineral—An example from the staurolite-grade metapelites of NW Maine. *Am. Mineral.* **1985**, *70*, 1–15.
11. Mao, J.W.; Wang, P.A.; Wang, D.H.; Bi, C.S. The tracer of tourmaline for rock-forming and metallogenic environments and its applied conditions. *Geol. Rev.* **1993**, *39*, 497–507. [CrossRef]
12. Shaoyong, J.; Jimin, Y.; Pei, N. Tourmaline—A Sensitive Tracer for Petrogenesis and Minerogenesis. *Geol. Rev.* **2000**, *46*, 594–604. [CrossRef]
13. Van Hinsberg, V.J.; Henry, D.J.; Marschall, H.R. Tourmaline: An ideal indicator of its host environment. *Can. Mineral.* **2011**, *49*, 1–16. [CrossRef]
14. Henry, D.J.; Dutrow, B.L. Tourmaline studies through time: Contributions to scientific advancements. *J. Geosci.* **2018**, *63*, 77–98. [CrossRef]
15. Marschall, H.R.; Altherr, R.; Kalt, A.; Ludwig, T. Detrital, metamorphic and metasomatic tourmaline in high-pressure metasediments from Syros (Greece): Intra-grain boron isotope patterns determined by secondary-ion mass spectrometry. *Contrib. Mineral. Pet.* **2008**, *155*, 703–717. [CrossRef]

16. Trumbull, R.B.; Krienitz, M.-S.; Gottesmann, B.; Wiedenbeck, M. Chemical and boron-isotope variations in tourmalines from an S-type granite and its source rocks: The Erongo granite and tourmalinites in the Damara Belt, Namibia. *Contrib. Mineral. Pet.* **2007**, *155*, 1–18. [CrossRef]
17. Balen, D.; Petrinec, Z. Contrasting tourmaline types from peraluminous granites: A case study from Moslavačka Gora (Croatia). *Mineral. Pet.* **2011**, *102*, 117–134. [CrossRef]
18. Yavuz, F.; Jiang, S.-Y.; Karakaya, N.; Karakaya, M.; Yavuz, R. Trace-element, rare-earth element and boron isotopic compositions of tourmaline from a vein-type Pb–Zn–Cu ± U deposit, NE Turkey. *Int. Geol. Rev.* **2011**, *53*, 1–24. [CrossRef]
19. Kalliomäki, H.; Wagner, T.; Fusswinkel, T.; Sakellaris, G. Major and trace element geochemistry of tourmalines from Archean orogenic gold deposits: Proxies for the origin of gold mineralizing fluids? *Ore Geol. Rev.* **2017**, *91*, 906–927. [CrossRef]
20. Zhang, M. Tourmaline Breccia Genesis and Hydrothermal Gold Deposits—Constrains from Chemical and B-Isotope Composition of Tourmaline. Ph.D. Thesis, China University of Geosciences (Beijing), Beijing, China, 2019. [CrossRef]
21. Zhao, L. Gemological-Mineralogical Characteristics and Genetic Analysis of "Ganlan" Jade in Ji'an, Jilin Province. Master's Thesis, China University of Geosciences (Beijing), Beijing, China, 2020. [CrossRef]
22. Sui, X. Study on Mineralogical Characteristics and Genesis of Phlogopites in "Ganlan Jade" Ore in Ji'an, Jilin. Master's Thesis, China University of Geosciences (Beijing), Beijing, China, 2021. [CrossRef]
23. Dutrow, B.L.; Henry, D.J. Petrogenetic utility of magnesian tourmaline: Extraordinary origin of everyday tourmaline. In Proceedings of the TUR2021 3rd International Conference on Tourmaline, Elba Island, Italy, 9–11 September 2021.
24. Song, B.; Nutman, A.P.; Liu, D.; Wu, J. 3800 to 2500 Ma crustal evolution in the Anshan area of Liaoning Province, northeastern China. *Precambrian Res.* **1996**, *78*, 79–94. [CrossRef]
25. Zhai, A.M.; Shen, B.F.; Yang, C.L.; Hu, X.D.; Cao, X.L.; Gong, X.H. Geological Evolvement and Ore-Forming of the Liaoning-Jilin Paleoproterozoic Rift. *Geol. Surv. Res.* **2005**, *28*, 213–220. [CrossRef]
26. Wang, H.C.; Ren, Y.W.; Lu, S.N.; Kang, J.L.; Chu, H.; Yu, H.B.; Zhang, C.J. Stratigraphic Units and Tectonic Setting of the Paleoproterozoic Liao–Ji Orogen. *Acta Geosci. Sin.* **2015**, *36*, 583–598. [CrossRef]
27. Wang, P.; Dong, Y.; Li, F.; Gao, B.; Gan, Y.; Chen, M.; Xu, W. Paleoproterozoic granitic magmatism and geological significance in Huanghuadian area, eastern Liaoning Province. *Acta Petrol. Sin.* **2017**, *33*, 2708–2724.
28. Hao, D.F.; Li, S.Z.; Zhao, G.C.; Sun, M.; Han, Z.Z.; Zhao, G.T. Origin and its constraint to tectonic evolution of Paleoproterozoic granitoids in the eastern Liaoning and Jilin province, North China. *Acta Petrol. Sin.* **2004**, *20*, 108–115. [CrossRef]
29. Meng, E.; Wang, C.-Y.; Yang, H.; Cai, J.; Ji, L.; Li, Y.-G. Paleoproterozoic metavolcanic rocks in the Ji'an Group and constraints on the formation and evolution of the northern segment of the Jiao-Liao-Ji Belt, China. *Precambrian Res.* **2017**, *294*, 133–150. [CrossRef]
30. Qin, Y. Geochronological Constraints on the Tectonic Evolution of the Liao-Ji Paleoproterozoic Rift Zone. Ph.D. Thesis, Jilin University, Changchun, China, 2013.
31. Li, X. Metamorphic Evolution and Genesis of The Ji'an Group in The Tonghua Region, Jilin Province. Master's Thesis, China University of Geosciences (Beijing), Beijing, China, 2016.
32. Shen, B.; Zhang, K.; Bi, J. Geological characteristics of double metallogenic belts in Paleoproterozoic Liaoji active belt. *Miner. Depos.* **2020**, *39*, 1–18.
33. Lu, X.-P.; Wu, F.-Y.; Guo, J.-H.; Wilde, S.A.; Yang, J.-H.; Liu, X.-M.; Zhang, X.-O. Zircon U–Pb geochronological constraints on the Paleoproterozoic crustal evolution of the Eastern block in the North China Craton. *Precambrian Res.* **2006**, *146*, 138–164. [CrossRef]
34. Yang, S.Y.; Jiang, S.Y.; Mao, Q.; Chen, Z.Y.; Rao, C.; Li, X.L.; Li, W.C.; Yang, W.Q.; He, P.L.; Li, X. Electron Probe Microanalysis in Geosciences: Analytical Procedures and Recent Advances. *At. Spectrosc.* **2022**, *43*, 186–200. [CrossRef]
35. Hawthorne, F.C.; Henrys, D.J. Classification of the minerals of the tourmaline group. *Eur. J. Mineral.* **1999**, *11*, 201–216. [CrossRef]
36. Bosi, F.; Lucchesi, S. Crystal chemistry of the schorl-dravite series. *Eur. J. Mineral.* **2004**, *16*, 335–344. [CrossRef]
37. Henry, D.J.; Novák, M.; Hawthorne, F.C.; Ertl, A.; Dutrow, B.L.; Uher, P.; Pezzotta, F. Nomenclature of the tourmaline-supergroup minerals. *Am. Mineral.* **2011**, *96*, 895–913. [CrossRef]
38. Henry, D.; Dutrow, B. Tourmaline at diagenetic to low-grade metamorphic conditions: Its petrologic applicability. *Lithos* **2012**, *154*, 16–32. [CrossRef]
39. Ertl, A.; Henry, D.J.; Tillmanns, E. Tetrahedral substitutions in tourmaline: A review. *Eur. J. Mineral.* **2018**, *30*, 465–470. [CrossRef]
40. Henry, D.J.; Dutrow, B.L. Tourmaline crystallography, crystal chemistry and nomenclature: Current status. In Proceedings of the TUR2021 3rd International Conference on Tourmaline, Elba Island, Italy, 9–11 September 2021.
41. Jiang, S.-Y.; Palmer, M.R.; Yeats, C.J. Chemical and boron isotopic compositions of tourmaline from the Archean Big Bell and Mount Gibson gold deposits, Murchison Province, Yilgarn Craton, Western Australia. *Chem. Geol.* **2002**, *188*, 229–247. [CrossRef]
42. Boynton, W.V. Cosmochemistry of the rare earth elements meteorite studies. In *Rare Earth Element Geochemistry*; Elsevier: Amsterdam, The Netherlands, 1984; pp. 63–114.
43. Van Hinsberg, V.J.; Henry, D.J.; Dutrow, B.L. Tourmaline as a Petrologic Forensic Mineral: A Unique Recorder of Its Geologic Past. *Elements* **2011**, *7*, 327–332. [CrossRef]
44. McDonough, W.F.; Sun, S.S. The composition of the Earth. *Chem. Geol.* **1995**, *120*, 223–253. [CrossRef]
45. Ertl, A.; Bačík, P. Considerations About Bi and Pb in the Crystal Structure of Cu-Bearing Tourmaline. *Minerals* **2020**, *10*, 706. [CrossRef]

46. Vereshchagin, O.S.; Wunder, B.; Britvin, S.N.; Frank-Kamenetskaya, O.V.; Wilke, F.D.; Vlasenko, N.S.; Shilovskikh, V.V. Synthesis and crystal structure of Pb-dominant tourmaline. *Am. Mineral.* **2020**, *105*, 1589–1592. [CrossRef]
47. Jiang, S.-Y.; Radvanec, M.; Nakamura, E.; Palmer, M.; Kobayashi, K.; Zhao, H.-X.; Zhao, K.-D. Chemical and boron isotopic variations of tourmaline in the Hnilec granite-related hydrothermal system, Slovakia: Constraints on magmatic and metamorphic fluid evolution. *Lithos* **2008**, *106*, 1–11. [CrossRef]
48. Ren, L.; Liu, X. Tourmaline and Its Relationship with Metamorphism, Zhongshan Station, Antarctica. *Acta Petrol. Mineral.* **1994**, *13*, 169–174.
49. Harlow, G.E.; Sorensen, S.S. Jade (Nephrite and Jadeitite) and Serpentinite: Metasomatic Connections. *Int. Geol. Rev.* **2005**, *47*, 113–146. [CrossRef]
50. Yu, H.; Yang, X. Geochemical characteristics, metallogenetic resource and processes of jasper from the world's major producer. *J. Guilin Univ. Technol.* **2019**, *39*, 311–320.